Dynamic wall modeling for LES of complex turbulent flows

By Meng Wang

1. Motivation and objectives

Large-eddy simulation (LES) of wall-bounded flows becomes prohibitively expensive at high Reynolds numbers if one attempts to resolve the small but dynamically important vortical structures (streaks) in the near-wall region. The number of grid points required scales as the square of the friction Reynolds number (Baggett, Jiménez & Kravchenko 1997), which is nearly the same as for direct numerical simulation (DNS). To circumvent the severe near-wall resolution requirement, LES can be combined with a wall-layer model. In this approach, LES is conducted on a relatively coarse grid designed to resolve the desired outer flow scales. The dynamic effects of the energy-containing eddies in the wall layer (viscous and buffer regions) are determined from a wall model calculation, which provides to the outer flow LES a set of approximate boundary conditions, often in the form of wall shear-stresses. Wall models which supply wall stresses to the LES are also called wall stress models.

The simplest wall stress models are analogous to the wall functions commonly used in Reynolds-averaged Navier-Stokes (RANS) approaches except that they are applied in an instantaneous sense in time-accurate calculations. The wall function provides an algebraic relationship between the local wall stresses and the tangential velocities at the first off-wall velocity nodes. This approach was first employed in a channel flow simulation by Schumann (1975), who assumed that the streamwise and spanwise velocity fluctuations are in phase with the respective surface shear stress components. A number of modifications to Schumann's model have been made by, for example, Grötzbach (1987) and Werner & Wengle (1991) to eliminate the need for *a priori* prescription of the mean wall shear stress and to simplify computations, and by Piomelli *et al.* (1989) to empirically account for the phase shift between the wall stress and near-wall tangential velocity due to the tilting of near-wall eddies. See Cabot & Moin (2000) and Nicoud *et al.* (2000) and the references therein for a review of the various wall stress models.

The algebraic wall stress models mentioned above all imply the logarithmic (power) law of the wall for the mean velocity, which is not valid in many complex flows. To incorporate more physics into the model, wall stress models based on boundary layer approximations have been proposed in recent years (Balaras, Benocci & Piomelli 1996; Cabot 1995; Cabot & Moin 2000). In this method, turbulent boundary-layer equations are solved numerically on an embedded near-wall mesh to compute the wall stress. These equations are forced at the outer boundary by the tangential velocities from LES, while no-slip conditions are applied at the wall. The turbulent eddy viscosity is modeled by a RANS type model, such as the mixing-length model with wall damping. Reasonable success has been achieved in predicting attached flows and flows with fixed separation points, such as the backward facing step flow. Cabot & Moin (2000) found that, in the case of the backward facing step, improved solutions were obtained when the mixing-length eddy viscosity was lowered from the standard RANS value. A dynamic procedure was suggested to determine the suitable model coefficient.

The present work is concerned with the use of wall models in the LES of complex turbulent flows with strong favorable/adverse pressure gradients and incipient separation. The wall model based on turbulent boundary layer equations (Cabot & Moin 2000) is employed and extended to carry out LES of boundary layer flows past an asymmetric trailing-edge shown in Fig. 1. The results are compared with those from the full LES with resolved wall-layers (Wang & Moin 2000) and the experimental measurements of Blake (1975). In particular, we are interested in determining the predictive capabilities of this hybrid LES/wall-modeling approach for flow separation, surface pressure fluctuations, and aerodynamic noise.

It will be shown that the LES with wall modeling procedure can result in drastic savings in computational cost with minimal degradation of flow statistics compared with the fully resolved LES. The wall model based on boundary layer equations and dynamically adjusted eddy viscosity is considerably more superior to its simpler variants based on the instantaneous log law. A main objective of this article is to highlight the need for reducing the value of RANS eddy viscosity when it is used in the LES context, which has not been emphasized enough by Cabot & Moin (2000). We will show that this is important for all flows, particularly attached flows. A modified dynamic procedure is used to determine the mixing-length model coefficient, and the simulation results are found to be in very good agreement with those from the full LES.

2. Results

2.1. *The trailing-edge flow*

The flow configuration is shown in Fig. 1, which depicts contours of the mean streamwise velocity of turbulent boundary layer flows past an asymmetric trailing-edge as computed by Wang & Moin (2000) using standard LES with wall resolution. This trailing-edge flow was originally studied experimentally by Blake (1975). The chord Reynolds number is 2.15×10^6, and the trailing-edge tip-angle is 25 degrees. In the numerical simulation, only the aft section (approximately 38% chord) of the model airfoil and the near wake are included in the computational domain, and the inlet Reynolds numbers based on the local momentum thickness and boundary-layer edge velocity are 2760 on the lower side and 3380 on the upper side. These values, obtained from an auxiliary RANS calculation, are used to duplicate the experimental conditions at the LES inflow station, although some questions remain concerning their fidelity. Details of the trailing-edge LES can be found in Wang & Moin (2000).

The complexity of the flow is best illustrated in Fig. 2, which plots the distributions of the mean pressure coefficient C_p (solid line) and skin-friction coefficient C_f ($\times 100$, dashed line) along the upper surface of the trailing-edge. Distributions along the lower surface, which is flat, resemble those of a flat plate boundary-layer and are thus not plotted. As the flow approaches the trailing-edge, it first experiences favorable pressure gradient, causing flow acceleration and increased skin friction. A region of adverse pressure gradient ensues, leading to flow deceleration and eventually unsteady separation. The skin friction decreases and becomes negative in the separated zone near the tip of the trailing-edge. It is worth noting that the discontinuous slope at the skin friction peak corresponds to the intersection of the flat surface with a circular arc (hence a discontinuity in surface curvature). Given the presence of strong favorable/adverse pressure gradients and flow separation, and the complex response of the skin friction, this flow provides a challenging test case to evaluate the predictive capabilities of wall models.

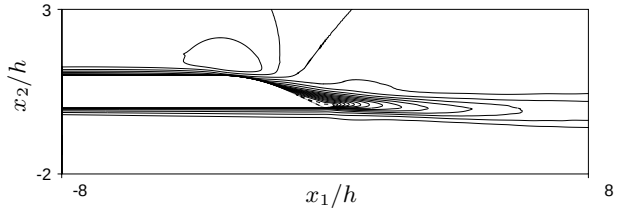

FIGURE 1. Boundary-layer flow past a trailing-edge. The contours (-0.081 to 1.207 with increment 0.068) represent the mean streamwise velocity normalized by the free-stream value (from Wang & Moin 2000).

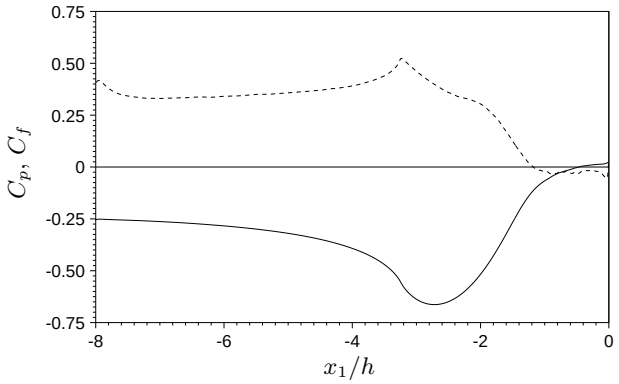

FIGURE 2. Distributions of the mean pressure and skin-friction coefficients along the upper surface: ——— C_p; - - - - $C_f \times 10^2$.

2.2. *Simulation method*

The same energy-conserving finite difference scheme with dynamic subgrid-scale (SGS) stress model used for the wall-resolved LES (Wang & Moin 2000) is employed. The computational domain is also identical to that of the full LES. It is of size $16.5h$, $41h$, and $0.5h$, where h denotes the airfoil thickness in the streamwise (x_1), wall-normal (x_2 or y), and spanwise (x_3) directions, respectively. The grid is coarsened to $768 \times 64 \times 24$, 1/6 of the original number of points. The first off-wall velocity nodes (on staggered mesh) are located at the lower edge of the logarithmic layer ($x_2^+ \approx 60$ for u_2 and $x_2^+ \approx 30$ for u_1 and u_3) near the computational inlet. The new grid is chosen to resolve the desired flow scales in the outer layer and is thus not strongly dependent on the Reynolds number. The total reduction in CPU time, due to both the smaller number of grid points and larger time steps, is over 90% compared to the full LES.

Since the simulation does not resolve the viscous sublayer, approximate wall boundary conditions are needed. They are imposed in terms of wall shear stress components τ_{wi} ($i = 1, 3$) determined from wall models of the form (Balaras *et al.* 1996; Cabot & Moin 2000)

$$\frac{\partial}{\partial x_2}\left(\nu + \nu_t\right)\frac{\partial u_i}{\partial x_2} = F_i, \qquad i = 1, 3, \tag{2.1}$$

where

$$F_i = \frac{1}{\rho}\frac{\partial p}{\partial x_i} + \frac{\partial u_i}{\partial t} + \frac{\partial}{\partial x_j}u_i u_j. \tag{2.2}$$

The eddy viscosity ν_t is obtained from a RANS type mixing-length eddy viscosity model

with near-wall damping (Cabot & Moin 2000):

$$\frac{\nu_t}{\nu} = \kappa y_w^+ \left(1 - e^{-y_w^+/A}\right)^2, \tag{2.3}$$

where $y_w^+ = y_w u_\tau/\nu$ is the distance to the wall in wall units (based on the local instantaneous friction velocity u_τ), κ is the model coefficient, and $A = 19$. The pressure in (2.2) is assumed x_2-independent, equal to the value from the outer-flow LES solution. Eqs. (2.1) and (2.2) are required to satisfy no-slip conditions on the wall and match the outer layer solutions at the first off-wall LES velocity nodes: $u_i = u_{\delta i}$ at $x_2 = \delta$.

Two simpler variants of the above wall model, with $F_i = 0$ and $F_i = \frac{1}{\rho}\frac{\partial p}{\partial x_i}$, have been considered previously (Wang 1999). These two cases, called equilibrium stress balance models (without and with pressure gradient), are particularly easy to implement since (2.1) can be integrated to give a closed-form expression for τ_{wi}.

In the general case, however, the boundary layer equations (2.1)–(2.3) have to be solved numerically to obtain u_1 and u_3, and hence τ_{w1} and τ_{w3}. They are integrated in time along with the outer flow LES equations, using the same numerical scheme (fractional step in combination with the Crank-Nicolson method for the diffusion term and third order Runge-Kutta scheme for convective terms). The wall-normal velocity component u_2 is determined from the divergence-free constraint. Note that no pressure Poisson equation is required since pressure is assumed constant in the wall-normal direction. The grid for wall layer computation coincides with the LES grid in the wall-parallel directions. In the direction normal to the wall, 32 points are distributed uniformly between the airfoil surface and the first off-wall velocity nodes for LES, with resolution of $\Delta x_2^+ \approx 1$ near the inlet. The computational cost for solving the boundary layer equations is insignificant compared with that for the outer layer LES because (1) there is no need to solve the x_2-momentum equation and the pressure Poisson equation, and (2), more importantly, the equations are solved in locally orthogonal coordinates instead of the general curvilinear coordinates used for the LES.

2.3. *The effect of model coefficient*

A good indicator of wall model performance is the prediction of the mean skin friction coefficient, which is shown in Fig. 3. The simple stress balance models, with $F_i = 0$ and $F_i = \frac{1}{\rho}\frac{\partial p}{\partial x_i}$ (dashed and chain-dashed lines respectively) and $\kappa = 0.4$ (the von Kármán constant), predict well the skin friction coefficient C_f on the flat surfaces, but deviate significantly from the full LES solution (dotted line) downstream of the C_f peak, where the flow undergoes a favorable-to-adverse pressure gradient transition. This suggests that terms not included in the model, such as the convective terms, are important.

The skin friction coefficient computed using the full boundary layer equations (2.1)–(2.3) and the standard von Kármán constant $\kappa = 0.4$ shows improved qualitative trend (chain-dotted lines). However, the magnitude is overpredicted in most regions, particularly on the flat surface, by up to 20%. This overprediction can be explained as follows: If the streamwise component of (2.1) and (2.2) are integrated from the wall to $y = \delta$ and then time-averaged, one obtains

$$\overline{\tau}_{w1} = \mu \left.\frac{\partial U_1}{\partial x_2}\right|_{x_2=0} = \frac{\rho}{\int_0^\delta \frac{dy}{\nu+\nu_t}} \left\{ U_{\delta_1} - \frac{1}{\rho}\frac{\partial P}{\partial x_1}\int_0^\delta \frac{y dy}{\nu+\nu_t} - \int_0^\delta \frac{\int_0^y \frac{\partial}{\partial x_j}\overline{u_1 u_j} dy'}{\nu+\nu_t} dy \right\}. \tag{2.4}$$

Note that to facilitate the analysis, ν_t has been treated as constant in the time-averaging as a first approximation. The first term in the curly brackets, which is always posi-

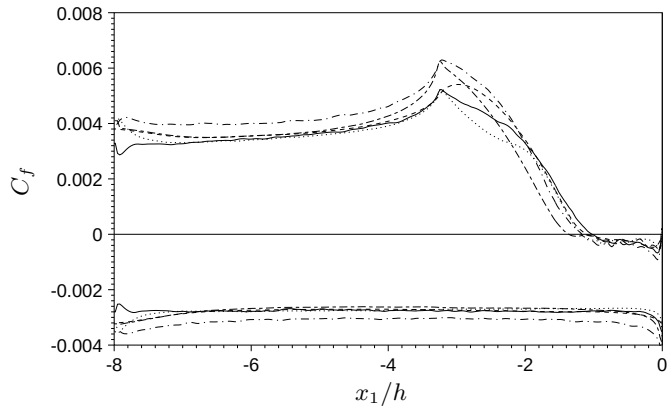

FIGURE 3. Distribution of the mean skin friction coefficient computed using LES with wall models given by (2.1). - - - - $F_i = 0$; — - — $F_i = \frac{1}{\rho}\frac{\partial p}{\partial x_i}$; — · — $F_i = \frac{1}{\rho}\frac{\partial p}{\partial x_i} + \frac{\partial u_i}{\partial t} + \frac{\partial}{\partial x_j}u_i u_j$ and $\kappa = 0.4$; ——— $F_i = \frac{1}{\rho}\frac{\partial p}{\partial x_i} + \frac{\partial u_i}{\partial t} + \frac{\partial}{\partial x_j}u_i u_j$ and dynamic κ; ····· full LES (no wall model).

tive, represents the wall shear stress from an equilibrium stress balance model without pressure gradient. The second term accounts for the mean pressure gradient effect, which contributes positively (negatively) to the wall shear stress under favorable (adverse) pressure gradient. The contribution from the nonlinear convective terms is represented by the last term in the brackets. This part, denoted by $\overline{\tau}^c_{w1}$, can be expanded to give

$$\overline{\tau}^c_{w1} = -\frac{\rho}{\int_0^\delta \frac{dy}{\nu+\nu_t}} \left\{ \int_0^\delta \frac{1}{\nu+\nu_t} \frac{\partial}{\partial x_1} \int_0^y \overline{u_1^2} dy' dy + \int_0^\delta \frac{\overline{u_1 u_2}}{\nu+\nu_t} dy \right\}. \tag{2.5}$$

The first term in (2.5) vanishes if the flow is homogeneous in the streamwise direction, such as in a turbulent channel flow. In the case of a flat-plate boundary layer with zero pressure gradient, it makes a positive, albeit small, contribution to the wall shear stress due to the thickening of the boundary layer. The dominant contribution to $\overline{\tau}^c_{w1}$ comes from the second term, which is positive for a flat plate boundary layer.

Thus we have shown mathematically that, at least on the flat section of the airfoil, the inclusion of the nonlinear terms in the wall model equation increases the wall stress, causing the overprediction shown in Fig. 3 if contributions from other terms in (2.4) are not altered. To offset this increase, the only option is to reduce the turbulent eddy viscosity ν_t and hence the multiplication factor before the curly brackets in (2.4). This mainly affects the equilibrium part of the wall stress (first term inside the brackets). The pressure-gradient and nonlinear parts of the wall stress are insensitive to ν_t because it appears both inside and outside the brackets with opposite effects.

The physical explanation for requiring lower ν_t, as pointed out by Cabot & Moin (2000), is the fact that the Reynolds stress carried by the nonlinear terms in the boundary layer equations is significant. Hence, instead of modeling the total stress as in typical RANS calculations, the eddy-viscosity model is expected to account for only the unresolved part of the Reynolds stress. Cabot & Moin (2000) suggested to compute the model coefficient dynamically by matching the stresses between the inner layer (wall model) and outer layer (LES) solutions. In the present case, since the horizontal grid is the same for both the LES and wall model calculations, and because the velocities are matched at the edge of the wall layer, the resolved portions of the nonlinear stresses from the

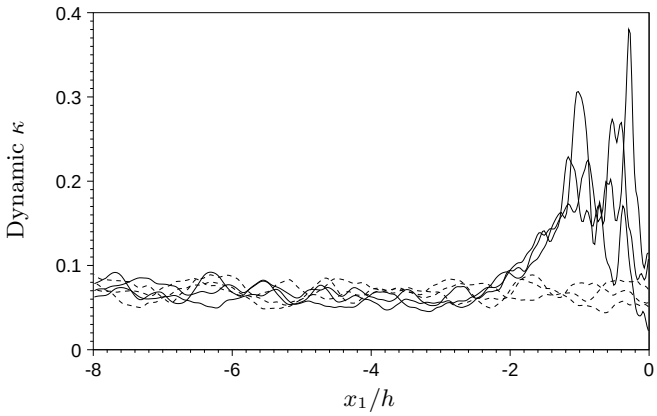

FIGURE 4. Dynamic κ for the mixing-length eddy viscosity model at three time instants. ——— upper side; - - - - lower side.

inner and outer layer calculations are the same. To match the unresolved portions of the stresses approximately, we equate the mixing-length eddy viscosity to the SGS eddy viscosity at the matching points, $\langle \nu_t \rangle = \langle \nu_{sgs} \rangle$, from which the model coefficient κ is extracted using (2.3). The averaging denoted by the angular brackets is performed in the spanwise direction as well as over the previous 150 time steps to obtain reasonably smooth data. One difficulty with this method is that ν_{sgs} is poorly behaved at the first off-wall velocity nodes because the velocities at the wall are not well defined (we used slip velocities extrapolated from the interior nodes to compute the strain rate tensor and ν_{sgs}). As a practical matter, the matching points for eddy viscosities are moved to the second layer of velocity nodes from the wall instead.

The dynamically computed κ at three time instants are exemplified in Fig. 4, where the solid lines represent those on the upper side and dashed lines on the lower side. They are found to be only a small fraction of the standard value of 0.4. This figure indicates that on average, on the flat surfaces, only less than 20% of the Reynolds stress is modeled by the mixing-length eddy viscosity. The rest is directly accounted for by the the nonlinear terms in the wall layer equations. By using the reduced, variable model coefficient κ, the computed skin friction coefficient is much improved, as demonstrated by the solid line in Fig. 3. This modeling approach gives the best overall agreement with the results of the resolved LES compared with other wall models tested.

2.4. *Comparisons with full LES solutions*

Comparisons of the velocity predictions using the wall modeling approach described above and those from the full LES (Wang & Moin 2000) show very good agreement. In Fig. 5 the velocity magnitude, defined as $U = (U_1^2 + U_2^2)^{1/2}$ and normalized by its value U_e at the boundary-layer edge, is plotted as a function of the vertical distance to the upper surface, at (from left to right) $x_1/h = -3.125$, -2.125, -1.625, -1.125, -0.625, and 0 (trailing-edge). With the exception of the trailing-edge point, these locations correspond to the measurement stations in Blake's (1975) experiment. The mean velocity profiles obtained with wall modeling (solid lines) agree extremely well with the full LES profiles (dashed lines) at all stations, including those in the separated region which starts at $x_1/h = -1.125$. The agreement between both computational solutions and the experimental data

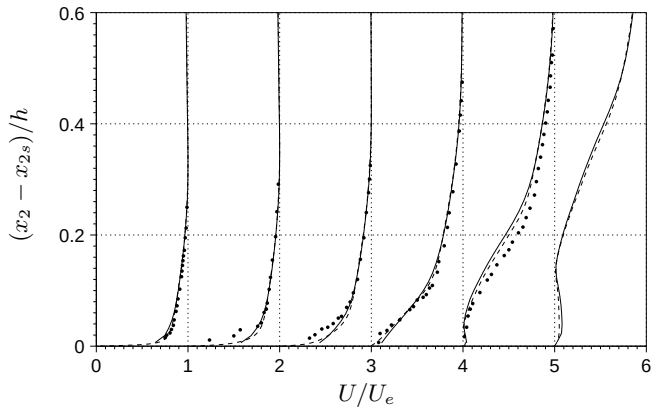

FIGURE 5. Profiles of the normalized mean velocity magnitude as a function of vertical distance to the upper surface, at (from left to right) $x_1/h = -3.125$, -2.125, -1.625, -1.125, -0.625, and 0 (trailing-edge). ——— LES with wall model; - - - - full LES; • Blake's experiment.

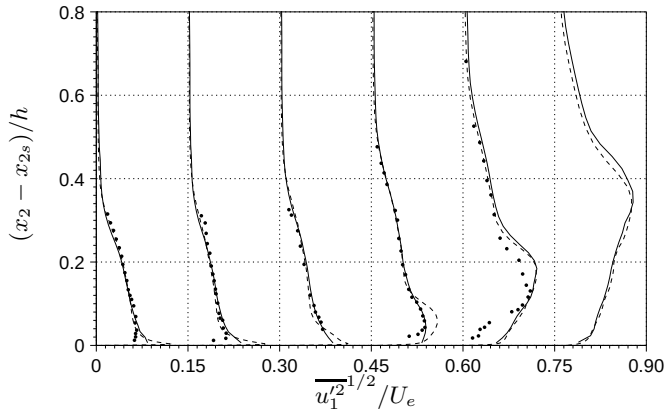

FIGURE 6. Profiles of the rms streamwise velocity fluctuations as a function of vertical distance from the upper surface, at (from left to right) $x_1/h = -4.625$, -2.125, -1.625, -1.125, -0.625, and 0 (trailing-edge). ——— LES with wall model; - - - - full LES; • Blake's experiment.

is also reasonable, and the potential reasons for the observed discrepancies have been discussed by Wang & Moin (2000).

Fig. 6 depicts the profiles of the rms streamwise velocity fluctuations at (from left to right) $x_1/h = -4.625$, -2.125, -1.625, -1.125, -0.625, and 0. Again, excellent agreement between the present solutions and those of the full LES is observed, with the notable exception at $x_1/h = -1.125$, where the wall model solution agrees (perhaps fortuitously) better with the experiment. It should be pointed out that the LES/wall-modeling predictions shown in Figs. 5 and 6 are significantly more accurate, judging from comparisons with the full LES data, than those reported by Wang (1999) using the simpler equilibrium stress balance models.

In Fig. 7 the mean streamwise velocity profiles (normalized by free-stream velocity U_∞) are compared at select near-wake stations $x_1/h = 0$, 0.5, 1.0, 2.0, and 4.0. The solid lines are obtained from the present simulation, and the dashed lines are from the full LES. The corresponding rms streamwise velocity fluctuations are depicted in Fig. 8. The

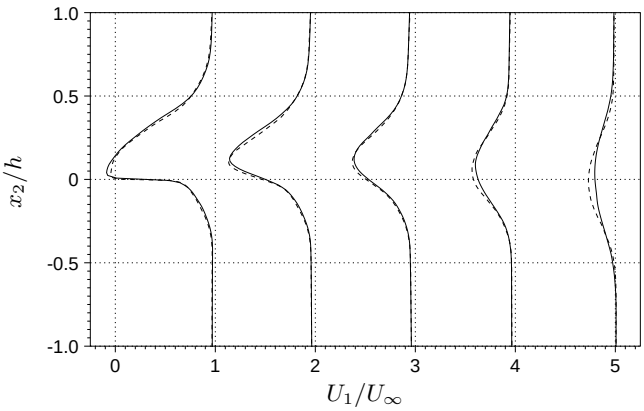

FIGURE 7. Profiles of the normalized mean streamwise velocity in the wake, at (from left to right) $x_1/h = 0$, 0.5, 1.0, 1.5, 2.0, and 4.0. ——— LES with wall model; – – – – full LES.

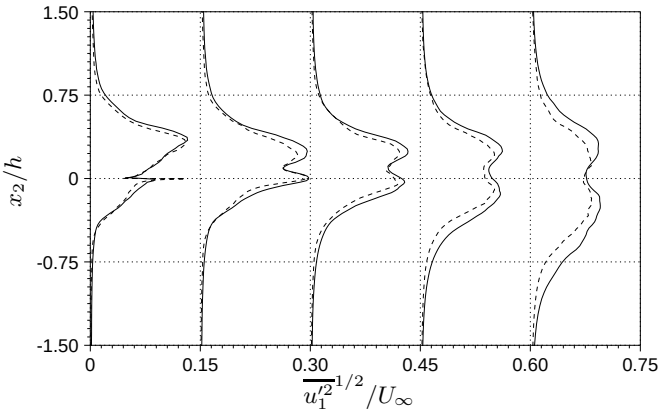

FIGURE 8. Profiles of the rms streamwise velocity fluctuations in the wake, at (from left to right) $x_1/h = 0$, 0.5, 1.0, 1.5, 2.0, and 4.0. ——— LES with wall model; – – – – full LES.

agreements between the LES solutions with and without wall modeling are good near the trailing-edge and deteriorate gradually in the downstream direction. This is caused by the much reduced grid resolution in the case of LES with wall modeling. The grid has been coarsened by the same factor in the wake as in the wall bounded region, even though the wall model does not play a role there. Apparently, this has caused insufficient grid resolution, particularly in the streamwise and spanwise directions.

Finally, Fig. 9 depicts the frequency spectra of surface pressure fluctuations obtained from LES in conjunction with the wall model and compares them with those from the full LES and Blake's experiment. The variable q_∞ used in the normalization is the dynamic pressure, defined as $\rho U_\infty^2/2$. Relative to the experimental data, the pressure spectra from the simulation employing the wall model are of comparable accuracy as those from the full LES, although the resolvable frequency ranges are narrower due to the coarser grid. However, relative to the full LES spectra, the spectral levels are somewhat overpredicted, particularly in the attached flow region (parts (a)–(c) of the figure). This phenomenon has also been observed previously in channel flow LES with wall models. The discrepancies, as pointed out by Wang (1999), may be attributable to the approximation of wall pressure

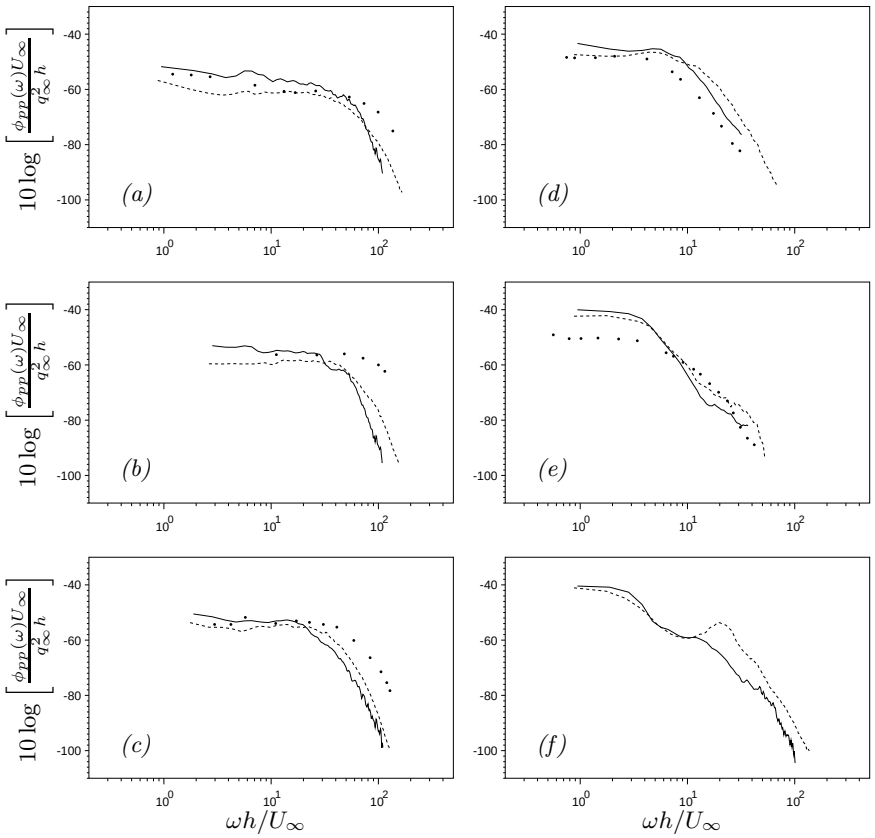

FIGURE 9. Frequency spectra of pressure fluctuations on the upper surface at $x_1/h =$ (a) -3.125, (b) -2.125, (c) -1.625, (d) -1.125, (e) -0.625, and (f) 0 (trailing-edge). ——— LES with wall model; – – – – full LES; • Blake's experiment.

by the cell-centered values adjacent to the wall and the fact that in the present LES formulation the "pressure" actually contains the subgrid-scale kinetic energy. The latter is negligibly small at the first off-wall pressure node if the wall layer is resolved but may not be negligible in the present case because of the coarse mesh. This issue needs to be examined in future investigations.

3. Conclusions and future work

In summary, we have developed a numerical procedure using a combination of LES with wall modeling for simulating complex wall-bounded flows. It is demonstrated that when a RANS type eddy viscosity is used in wall-layer equations that contain nonlinear convective terms, its value must be reduced to account for only the unresolved part of the Reynolds stress. A dynamically adjusted wall-model eddy viscosity is employed in the LES of turbulent boundary layer flows past an asymmetric trailing-edge. The method is shown to predict low-order velocity statistics in very good agreement with those from the full LES and at less than 10% of the original computational cost. In particular, the unsteady separation near the trailing-edge is predicted correctly. This cost-effective approach will be very useful for simulating the high Reynolds number trailing-edge ex-

periment currently underway in the Navy's large cavitation channel (Bourgoyne, Ceccio & Dowling 2000) and for shape optimization in order to achieve passive noise control. The latter two items are among the planned activities as an extension of the present trailing-edge aeroacoustics project. In addition, we will continue to develop improved approximate wall boundary conditions for LES applications and critically evaluate their impact on the predictions of unsteady surface pressure and radiated noise.

Acknowledgments

This research was supported by ONR Grant N00014-95-1-0221. We would like to thank P. Bradshaw, W. Cabot, and J. Jiménez for valuable discussions during the course of this work.

REFERENCES

Baggett, J. S., Jiménez, J. & Kravchenko, A. G. 1997 Resolution requirements in large-eddy simulations of shear flows. *Annual Research Briefs*, Center for Turbulence Research, NASA Ames/Stanford Univ. 51-66.

Balaras, E., Benocci, C. & Piomelli, U. 1996 Two-layer approximate boundary conditions for large-eddy simulation. *AIAA J.* **34**, 1111-1119.

Blake, W. K. 1975 *A Statistical Description of Pressure and Velocity Fields at the Trailing Edge of a Flat Strut.* DTNSRDC Report 4241, David Taylor Naval Ship R & D Center, Bethesda, Maryland.

Cabot, W. 1995 Large-eddy simulations with wall-models. *Annual Research Briefs*, Center for Turbulence Research, NASA Ames/Stanford Univ. 41-50.

Cabot, W. & Moin, P. 2000 Approximate wall boundary conditions in the large-eddy simulation of high Reynolds number flow. *Flow Turb. Combust.* **63**, 269-291.

Bourgoyne, D., Ceccio, S. & Dowling, D. 2000 Hydrofoil trailing-edge hydrodynamics at high Reynolds numbers. *ONR Turbulence and Wake Review 2000*, Tucson, Arizona.

Grötzbach, G. 1987 Direct numerical and large eddy simulation of turbulent channel flows. In *Encyclopedia of Fluid Mechanics*, Cheremisinoff, N. P. ed., Gulf Pub. Co., Chap. 34. 1337-1391.

Nicoud, F., Baggett, J. S., Moin, P. & Cabot, W. 2000 LES wall modeling based on suboptimal control theory. To appear *in Phys. Fluids.*

Piomelli, U., Ferziger, J., Moin, P. & Kim, J. 1989 New approximate boundary conditions for large eddy simulations of wall-bounded flows. *Phys. Fluids.* **1**, 1061-1068.

Schumann, U. 1975 Subgrid scale model for finite difference simulations of turbulent flows in plane channels and annuli. *J. Comp. Phys.* **18**, 376-404.

Wang, M. 1999 LES with wall models for trailing-edge aeroacoustics. *Annual Research Briefs*, Center for Turbulence Research, NASA Ames/Stanford Univ. 355-364.

Wang, M. & Moin, P. 2000 Computation of trailing-edge flow and noise using large-eddy simulation. *AIAA J.* **38**, 2201-2209.

Werner, H. & Wengle, H. 1991 Large eddy simulation of turbulent flow over and around a cube in a plane channel. In *Proc. Eighth Symp. Turb. Shear Flows.* 1941-1946.